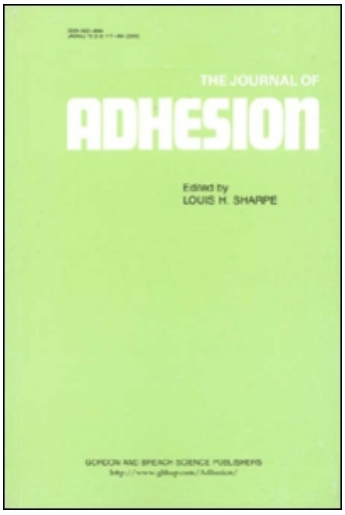

The Journal of Adhesion
Publication details, including instructions for authors and subscription information:
http://www.informaworld.com/smpp/title~content=t713453635

Stress Analysis of Generally Asymmetric Single Lap Adhesively Bonded Joints

Jungmin Lee[a]; Hyonny Kim[a]
[a] School of Aeronautics and Astronautics, Purdue University, West Lafayette, Indiana, USA

To cite this Article Lee, Jungmin and Kim, Hyonny(2005) 'Stress Analysis of Generally Asymmetric Single Lap Adhesively Bonded Joints', The Journal of Adhesion, 81: 5, 443 — 472
To link to this Article: DOI: 10.1080/00218460590944918
URL: http://dx.doi.org/10.1080/00218460590944918

The Journal of Adhesion, 81:443–472, 2005

ISSN: 0021-8464 print/1545-5823 online
DOI: 10.1080/00218460590944918

Taylor & Francis
Taylor & Francis Group

Stress Analysis of Generally Asymmetric Single Lap Adhesively Bonded Joints

Jungmin Lee
Hyonny Kim
School of Aeronautics and Astronautics, Purdue University, West Lafayette, Indiana, USA

An analysis is presented that predicts shear and peel stresses in an adhesively bonded single lap joint having general asymmetric configuration. The single lap joint is under tension loading together with moments induced by geometric eccentricity. Because these eccentricity moments are the key elements of this analysis, a general relationship between the eccentricity moments and simple geometric moments has been determined with the aid of finite element analysis (FEA). Example calculations show that the shear- and peel-stress profiles from the closed-form model are well matched to FEA results except in the small regions near the free ends of the joints, because of the shear lag basis of the model. For asymmetric joints, the model predictions are more accurate for the case of modulus eccentricity than thickness eccentricity. Elastic-limit load predictions accounting for both shear and peel stress in the adhesive have been used to find optimal joint configurations between asymmetric adherends.

Keywords: Asymmetric joint; Shearlag; Beam on elastic foundation; Elastic limit load

NOMENCLATURE

c = half overlap length of joint
D_i = bending stiffness of adherends
E_a = Young's modulus of adhesive
E_i = Young's modulus of adherends
Error 1, Error 2 = error function 1 and 2
G_a = shear modulus of adhesive
k = spring constant for beam on elastic foundation, see Eq. 13

Received 8 August 2004; in final form 7 January 2005.

Address correspondence to Hyonny Kim, School of Aeronautics and Astronautics, Purdue University, 315 N, Grant Street, West Lafayette, IN 47907, USA. E-mail: hyonny@ecn.purdue.edu

M_i = internal moment resultants in adherends
$\overline{M}_i$ = moment boundary conditions, see Eqs. 21 and 24
$\overline{M}_{\text{TOT}}$ = total moment, $\overline{M}_{\text{TOT}} = |\overline{M}_1| + |\overline{M}_2|$
N_f = failure load at elastic limit of adhesive
N_i = internal in-plane axial stress resultants in adherends
N_x = external tension loading applied to joint
Q_i = internal transverse shear resultants in adherends
$\overline{Q}_i$ = shear boundary conditions, see Eq. 22 and 25
t_a = thickness of adhesive
t_i = thickness of adherends
u_i = in-plane displacement component in adherends
w_i = out-of-plane displacement component in adherends
$\tilde{w}$ = relative out-of-plane displacements, $\tilde{w} = w_1 - w_2$
x = longitudinal coordinate
z_i = transverse coordinate in adherends
β = beam on elastic foundation stiffness constant, see Eq. 16
γ_a = shear strain in adhesive
Δ = ratio of $\overline{M}_1$ over $\overline{M}_{\text{TOT}}$
ε_{xi} = in-plane extensional strain in adherends
η = geometric and material constants, see Eq. 38
λ = geometric and material constants, see Eq. 37
ξ = eccentricity-geometric moment conversion factor, see Eq. 55
σ_p = peel stress at adherend-bond interface
τ_a = shear stress in adhesive
τ_{ave} = average adhesive shear stress
τ_y = yield stress of adhesive

Subscript

i = adherend 1 or 2

INTRODUCTION

A closed-form model is developed that predicts shear and peel stresses in adhesively bonded single lap joints loaded by both in-plane tension force and by moments induced from the geometric eccentricity of the joint. This model computes shear stress based on shear lag assumptions and predicts peel stress using a beam on elastic foundation (BOEF) approach. By accounting for the coupling of peel stress terms within the shear governing equation, this model permits the stress analysis of general asymmetric joints, that is, joints that have adherends of mismatched elastic modulus and thickness.

Classical analyses, based on shear lag, have been previously developed to predict only the adhesive shear stress in bonded joints of uniform bondline thickness for a symmetric joint with tension load only [1, 2]. Improvements to the classical model include predicting peel stress and edge moments in single lap joints [3–6], accounting for plasticity in the adhesive prior to failure [7, 8], and allowing for transverse shear deformation of the symmetric adherends [9]. Kim [10] has extended the classical model to predict the effects of bondline thickness variation along the overlap dimension.

When the joint is simplified to a symmetric joint, the shear and peel governing equations are fully decoupled and the edge moments can be calculated from simple geometry of the joint. Thus, Goland and Reissner [3] assumed a uniform rotation of the symmetric joint with corresponding edge moments. Ojalvo and Eidinoff [4] and Oplinger [5] derived coupled governing equations based on plate theory in the manner first introduced by Goland and Reissner [3] and noticed that the joint rotates nonlinearly as a function of the applied tension load. This rotation of the joint should be accounted for when calculating the moment boundary conditions (defined as edge moments); however, only the symmetric joint case was analyzed and edge moments were calculated based on uniform joint rotation.

Kline [6] presented a general joint analysis theory that accounts for asymmetry of the joint, but only a symmetric joint was analyzed. Delale, Erdogan, and Aydinoglu [11] extended Goland and Reissner's approach for symmetric joints by formulating the adhesive shear stress equation to account for asymmetric adherends. For the asymmetric single lap joint, Delale, Erdogan, and Aydinoglu [11] suggest that the eccentricity moment boundary conditions acting on the both ends of the single lap joint can be calculated as a simple multiplication of tension loading and geometric eccentricity of the joint, and that the moments have the same magnitude but opposite direction. With the suggested moment boundary conditions previously described, the authors of the present work have found that the resulting adhesive shear-stress profile will not satisfy force equilibrium with the applied tension load. Similar approaches for the asymmetric joints are presented by Yang and Pang [12], Bigwood and Crocombe [13], Mortensen and Thomson [14], and Wu, Romeijn, and Wardenier [15], but no closed-form solution was successfully derived for the generally asymmetric case, with boundary conditions defined such that the predicted shear-stress profile equilibrates with the applied loading. In these papers, the edge moments are treated as known input parameters.

Tong [16] established peel and shear governing equations based on equilibrium of the asymmetric joint. Strain energy release rate

was calculated from those equations to predict failure only for the symmetric case, however, and thus the asymmetric problem was left unsolved (in closed form). Fernlund *et al.* [17] computed critical energy release rate as a function of the mode of loading for the cracked lap shear joint, single lap shear joint, and double strap joint. Moments at both ends of the joint were treated as known input parameters and failure load of the joint is compared with experimental results. Adams [18] reviewed classical linear closed-form solutions by Volkerson [1] and Goland and Reissner [3]. Improvements such as adding nonlinear material properties and accounting for realistic adhesive geometry were presented by the finite element method. Adams suggested that finite element analysis was the best way for treating nonlinear mechanics and material behavior in real joints.

To the authors' best knowledge, there are no closed-form analytical works that are applicable to generally asymmetric joints with combined tension loading and self-induced eccentricity moments whose stress solutions satisfy force equilibrium. A difficulty of this analysis lies in the definition of the moment boundary conditions. It is found that the moment boundary conditions simply calculated from the geometric eccentricity of the joint can yield adhesive stress profiles that do not satisfy force equilibrium. In this work, finite element analysis (FEA) that accurately predicts the shear- and the peel-stress profiles in bonded single lap joints are used to guide the development of analytical relationships between the geometrically calculated eccentricity moments, which can be known *a priori*, and moment boundary conditions that insure equilibrium of the stress profiles relative to the externally applied load.

MODEL DESCRIPTION

A general single lap joint with all relevant geometric parameters is shown in Figure 1. The only externally applied load is the in-plane force (per unit width), N_x. A differential element of the joint at any location x is shown in Figure 2 together with all internal stress and stress resultant quantities. The vertical axes z_1 and z_2 are defined from the bottom of adherends 1 and 2. The following assumptions are made for the single lap joint:

- adherends and adhesive have constant thickness,
- adhesive carries shear and peel stresses only,
- uniform shear- and peel-stress profiles through the adhesive thickness (z direction),

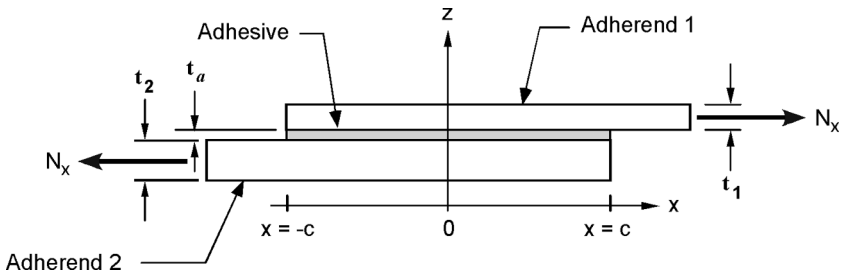

FIGURE 1 Adhesively bonded single lap joint.

- adherends do not deform because of transverse shear, and
- linear elastic material behavior.

Using Figure 2, the force and moment equilibrium equations of adherends 1 and 2 can be determined and are listed in Equations (1)–(6). Note that higher order terms in the moment equilibrium have been neglected:

$$\frac{dN_1}{dx} = \tau_a \tag{1}$$

$$\frac{dQ_1}{dx} = -\sigma_p \tag{2}$$

$$\frac{dM_1}{dx} = Q_1(x) + \frac{t_1}{2}\tau_a \tag{3}$$

$$\frac{dN_2}{dx} = -\tau_a \tag{4}$$

$$\frac{dQ_2}{dx} = \sigma_p \tag{5}$$

$$\frac{dM_2}{dx} = Q_2(x) + \frac{t_2}{2}\tau_a. \tag{6}$$

These relationships will be used throughout the derivation of governing equations for shear and peel stress components within the adhesive. Note that only the joint region is being modeled, $-c \leq x \leq c$. The extra adherend regions shown in Figure 1 are not accounted for when deriving governing equations for shear and peel stresses in the adhesive.

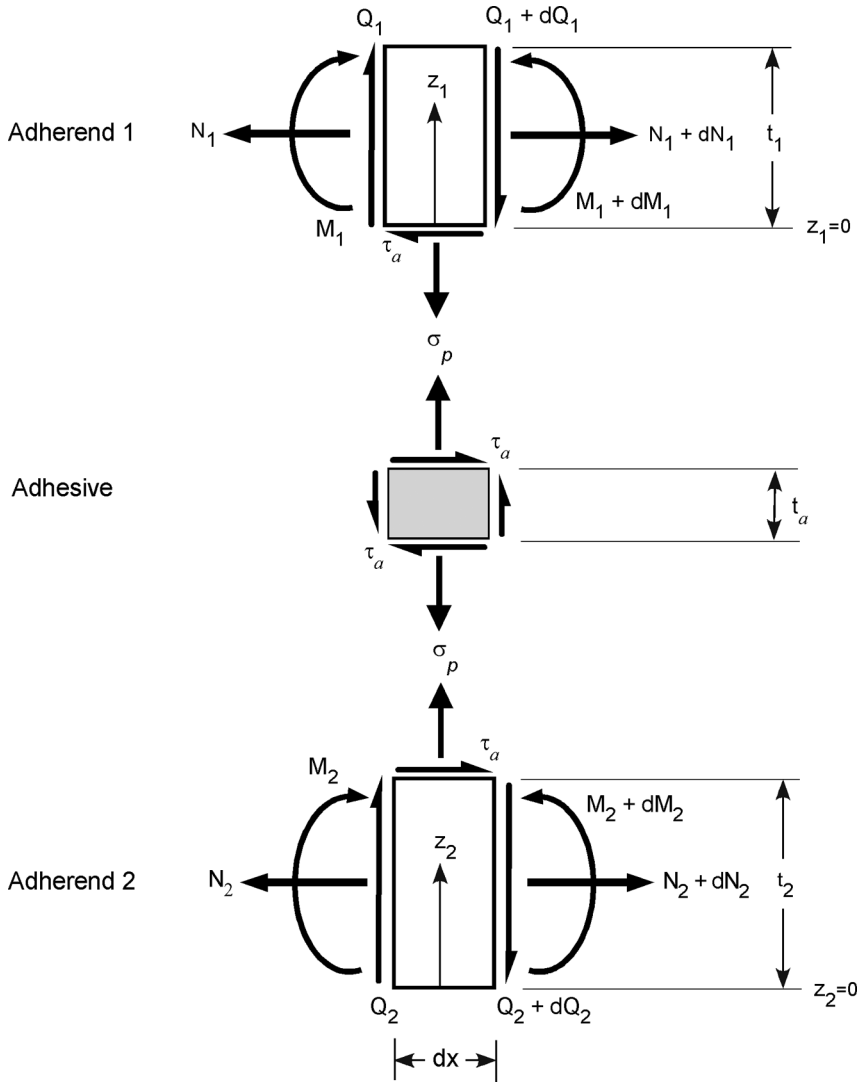

FIGURE 2 Differential element of single lap joint.

SHEAR STRESS

To determine shear stress distribution within the adhesive, the classical shear lag assumption has been adopted. The shear strain in the adhesive is determined from the relative in-plane displacements of

the adherends at the adhesive–adherend interfaces.

$$\gamma_a = \frac{1}{t_a}(u_1|_{z_1=0} - u_2|_{z_2=t_2}). \tag{7}$$

Differentiating Equation (7) with respect to x yields

$$\frac{d\gamma_a}{dx} = \frac{1}{t_a}(\varepsilon_{x1}|_{z_1=0} - \varepsilon_{x2}|_{z_2=t_2}) \tag{8}$$

where ε_{x1} and ε_{x2} are the longitudinal strains of adherends 1 and 2, respectively.

Both axial loading and bending moments are accounted for when constructing the longitudinal strain profile, ε_x, in each adherend.

$$\varepsilon_{x1} = \frac{N_1}{E_1 t_1} - \frac{M_1}{D_1}\left(z_1 - \frac{t_1}{2}\right), \quad 0 \le z_1 \le t_1 \tag{9}$$

$$\varepsilon_{x2} = \frac{N_2}{E_2 t_2} - \frac{M_2}{D_2}\left(z_2 - \frac{t_2}{2}\right), \quad 0 \le z_2 \le t_2 \tag{10}$$

where N_1 and N_2 are the in-plane axial stress resultants, M_1 and M_2 are the internal moment resultants, and D_1 and D_2 are the bending rigidity for the adherends 1 and 2, respectively. Note that the adhesive shear stress, τ_a, acting on the interfaces of the adhesive and the adherends (see Figure 2) is not accounted for in the bending contributions to the longitudinal strain component of each adherend.

Substituting Equations (9) and (10) into Equations (8) yields

$$\frac{d\gamma_a}{dx} = \frac{1}{t_a}\left(\frac{N_1}{E_1 t_1} - \frac{N_2}{E_2 t_2}\right) + \frac{1}{t_a}\left(\frac{M_1 t_1}{2D_1} + \frac{M_2 t_2}{2D_2}\right). \tag{11}$$

Differentiating Equation (11) with respect to x once more and substituting in Equations (1), (3), (4), and (6) yields the adhesive shear stress, τ_a, which can be written in terms of the adhesive shear strain, γ_a, and shear modulus, G_a, for a linear elastic adhesive.

$$\frac{d^2\gamma_a}{dx^2} = \frac{G_a}{t_a}\left[\left(\frac{1}{E_1 t_1} + \frac{1}{E_2 t_2}\right) + \frac{1}{4}\left(\frac{t_1^2}{D_1} + \frac{t_2^2}{D_2}\right)\right]\gamma_a + \frac{1}{2t_a}\left(\frac{t_1}{D_1}Q_1 + \frac{t_2}{D_2}Q_2\right) \tag{12}$$

Equation (12) is the governing equation of the shear strain in the adhesive. Note that this governing equation is coupled with transverse shear-stress resultants within the adherends, Q_1 and Q_2, which can be calculated from the beam transverse deflections upon solving for the peel-stress profile.

PEEL STRESS

To calculate peel stress, the single lap joint is modeled by two simple beams connected by a distributed elastic spring bed, as shown in Figure 3. The spring constant, k, is chosen as a combination of adhesive Young's modulus, E_a, and thickness of the adhesive, t_a:

$$k = \frac{E_a}{t_a}. \tag{13}$$

In this joint, the tension loading N_x produces a shear stress, $\tau_a(x)$, along the adherends and the adhesive interfaces. Also moments, $M_1(x)$ and $M_2(x)$ are induced through the adherends from the geometric eccentricity of the joint. These eccentricity bending moments are responsible for the peel stress component, $\sigma_p(x)$.

A fourth-order linear differential equation for the relative vertical displacement, $\tilde{w}$, based on beam-on-elastic-foundation (BOEF) interaction between the adherends, can be derived.

$$\frac{d^4\tilde{w}}{dx^4} + k\left(\frac{1}{D_1} + \frac{1}{D_2}\right)\tilde{w} = 0 \tag{14}$$

where $\tilde{w} = w_1 - w_2$ is the relative vertical displacement components of the adherends 1 and 2. Equation (14) is solved for the relative vertical displacement, $\tilde{w}$, by the general solution

$$\tilde{w}(x) = e^{\beta x}(C_1 \cos \beta x + C_2 \sin \beta x) + e^{-\beta x}(C_3 \cos \beta x + C_4 \sin \beta x) \tag{15}$$

where

$$\beta = \frac{1}{\sqrt{2}}\left[k\left(\frac{1}{D_1} + \frac{1}{D_2}\right)\right]^{1/4}. \tag{16}$$

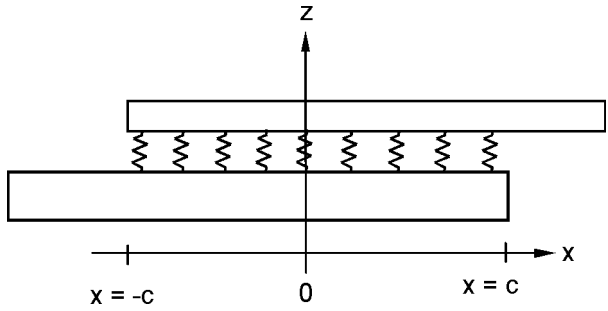

FIGURE 3 Beam on elastic foundation, peel stress model.

C_1 to C_4 are constants and can be found from boundary conditions of the joint. The peel stress can then be calculated from Equation (15) as

$$\sigma_p(x) = k\tilde{w} = k(w_1 - w_2). \tag{17}$$

BOUNDARY CONDITIONS

Four boundary conditions are needed to determine the four coefficients C_1 to C_4 in Equation (15). General boundary conditions of the joint are shown in Figure 4 and are presented in Equations (18)–(29).

At $x = -c$,

$$M_1(-c) = D_1 \frac{d^3 w_1}{dx^2} = 0, \tag{18}$$

$$Q_1(-c) = D_1 \frac{d^3 w_1}{dx^3} = 0, \tag{19}$$

$$N_1(-c) = 0, \tag{20}$$

$$M_2(-c) = D_2 \frac{d^2 w_2}{dx^2} = \overline{M}_2, \tag{21}$$

$$Q_2(-c) = D_2 \frac{d^3 w_2}{dx^3} = \overline{Q}_2, \tag{22}$$

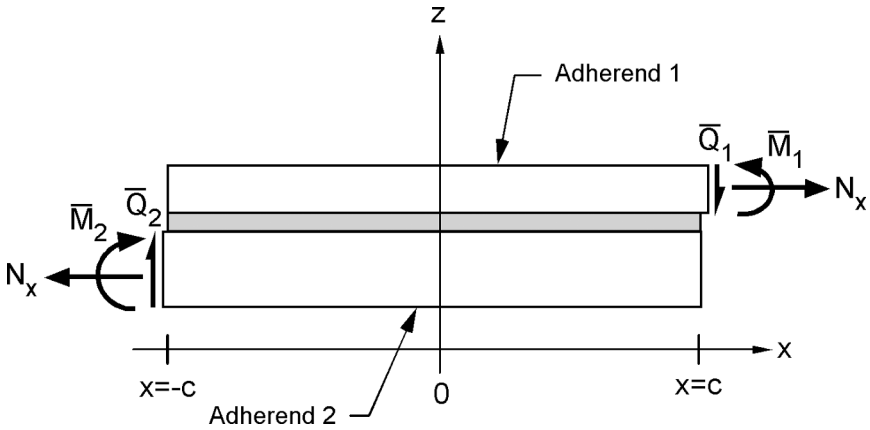

FIGURE 4 Single lap joint boundary conditions.

and

$$N_2(-c) = N_x. \tag{23}$$

At $x = c$,

$$M_1(c) = D_1 \frac{d^2 w_1}{dx^2} = \overline{M}_1, \tag{24}$$

$$Q_1(c) = D_1 \frac{d^3 w_1}{dx^3} = \overline{Q}_1, \tag{25}$$

$$N_1(c) = N_x, \tag{26}$$

$$M_2(c) = D_2 \frac{d^2 w_2}{dx^2} = 0, \tag{27}$$

$$Q_2(c) = D_2 \frac{d^3 w_2}{dx^3} = 0, \tag{28}$$

and

$$N_2(c) = 0. \tag{29}$$

Note that $\overline{Q}_1$, $\overline{Q}_2$, $\overline{M}_1$, and $\overline{M}_2$ depend on the specific boundary conditions at the ends of the joint and in general are not known *a priori*.

The boundary conditions in Equations (18)–(29) must be expressed in terms of the relative displacement, $\tilde{w}$, so as to be compatible with Equation (15).

At $x = -c$,

$$\left.\frac{d^2 \tilde{w}}{dx^2}\right|_{x=-c} = -\frac{\overline{M}_2}{D_2} \tag{30}$$

and

$$\left.\frac{d^3 \tilde{w}}{dx^3}\right|_{x=-c} = -\frac{\overline{Q}_2}{D_2}. \tag{31}$$

At $x = c$,

$$\left.\frac{d^2 \tilde{w}}{dx^2}\right|_{x=c} = \frac{\overline{M}_1}{D_1} \tag{32}$$

and

$$\left.\frac{d^3\tilde{w}}{dx^3}\right|_{x=c} = \frac{\overline{Q}_1}{D_1}. \tag{33}$$

SOLUTION PROCEDURE

The boundary conditions specified by Equations (30)–(33) are used to solve for the four coefficients C_1–C_4 in Equation (15). The assumption is now made that the left-hand side of the joint is fixed at $x = -c$, and the right hand side at $x = c$, can translate in the z direction but not rotate. These conditions are illustrated in Figure 5. Thus, $\overline{Q}_1$ and $\overline{Q}_2$ are zero but $\overline{M}_1$ and $\overline{M}_2$ are unknown because the chosen boundary conditions make the problem statically indeterminate. Real structures with significant unbonded length, for example, the thin skin of an aircraft in a single lap splice joint, would not have the transverse displacement constraint which exists when testing a lap joint in a test machine. Therefore, the transverse displacement was not confined. However, to preserve consistency of the loading direction, the condition of no rotation was enforced. This free translation with condition of no rotation results in a considerable moment reaction, producing larger shear and peel stresses in the joint than the case of fixed translation with free rotation (typically assumed in other works). Therefore, the chosen boundary conditions can be considered as conservative.

The substitution of Equation (15) into Equations (30)–(33) can be expressed as a system of linear equations from which the coefficients C_1–C_4 can be determined. This result is presented in compact form

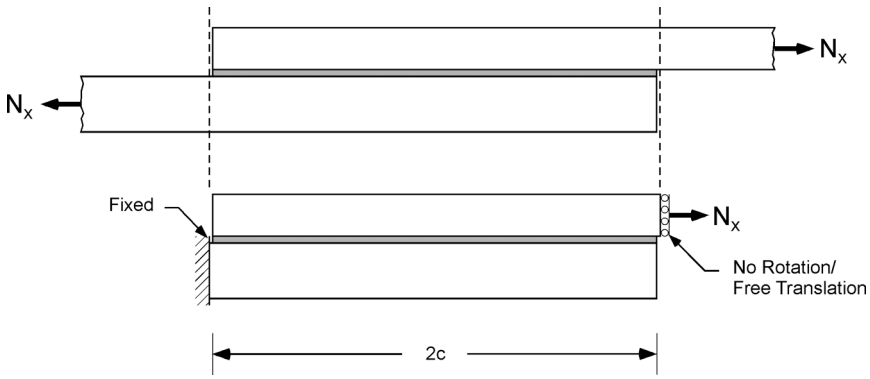

FIGURE 5 Single lap joint geometric constraints.

by the aid of the groupings of terms θ_1–θ_9, which are listed in the Appendix in Equations (A1)–(A9). The coefficients to Equation (15), C_1–C_4, are written in terms of θ_1–θ_9 and are listed in the Appendix in Equations (A10)–(A13).

Once the unknown moments $\overline{M}_1$ and $\overline{M}_2$ are determined, Equations (15) and (17) can be used to compute the peel stress in the adhesive. Recall the shear strain governing equation [Equation (12)] requires the internal transverse shear-force profiles in the adherends. These can be found by integrating Equations (2) and (5) with respect to x to get $Q_1(x)$ and $Q_2(x)$, which will be substituted into Equation (12),

$$Q_1(x) = -\int k\tilde{w}(x)dx + C_5 \tag{34}$$

and

$$Q_2(x) = \int k\tilde{w}(x)dx + C_6, \tag{35}$$

where C_5 and C_6 are integration constants and can be found from Equations (19) and (28) C_5 and C_6 are listed in the Appendix in Equations (A14) and (A15).

Substitute Equations (34) and (35) into Equation (12) to obtain the final shear-strain governing equation:

$$\frac{d^2\gamma_a}{dx^2} - \lambda^2\gamma_a = \eta\int k\tilde{w}(x)dx + \zeta \tag{36}$$

where

$$\lambda^2 = \frac{G_a}{t_a}\left[\left(\frac{1}{E_1t_1} + \frac{1}{E_2t_2}\right) + \frac{1}{4}\left(\frac{t_1^2}{D_1} + \frac{t_2^2}{D_2}\right)\right], \tag{37}$$

$$\eta = \frac{1}{2t_a}\left(\frac{t_1}{D_1} - \frac{t_2}{D_2}\right), \tag{38}$$

and

$$\zeta = \frac{1}{2t_a}\left(\frac{t_1}{D_1}C_5 + \frac{t_2}{D_2}C_6\right). \tag{39}$$

Equation (36) is a second-order ordinary differential equation with constant coefficients. The solution consists of a homogeneous and a particular solution:

$$\gamma_a(x) = \gamma_a^h + \gamma_a^p \tag{40}$$

The homogeneous solution is

$$\gamma_a^h(x) = C_7 \cosh(\lambda x) + C_8 \sinh(\lambda x). \tag{41}$$

The particular solution is

$$\begin{aligned}\gamma_a^p(x) = {} & e^{\beta x}[C_9 \cos(\beta x) + C_{10} \sin(\beta x)] \\ & + e^{-\beta x}[C_{11} \cos(\beta x) + C_{12} \sin(\beta x)] + C_{13}\end{aligned} \tag{42}$$

where C_7–C_{13} are constants. C_9–C_{13} are found by substituting Equation (42) into Equation (36) and comparing both sides. The end result is listed in the Appendix in Equations (A18) to (A22). The remaining unknown constants, C_7 and C_8, are determined using the in-plane force and moment boundary conditions listed within Equations (18)–(29). These can be expressed as gradients in shear strain using Eq. (11).

At $x = -c$,

$$\left.\frac{d\gamma_a}{dx}\right|_{x=-c} = -\frac{N_x}{E_2 t_2 t_a} + \frac{t_2}{2D_2 t_a}\overline{M}_2. \tag{43}$$

At $x = c$,

$$\left.\frac{d\gamma_a}{dx}\right|_{x=c} = \frac{N_x}{E_1 t_1 t_a} + \frac{t_1}{2D_1 t_a}\overline{M}_1. \tag{44}$$

The complete solution, Equation (40), should satisfy the transformed boundary conditions, resulting in the constants C_7 and C_8, which are listed in the Appendix as Equations (A16) and (A17).

Now, the shear-strain governing equation [Equation (12)] and the peel-stress governing equation [relative displacement $\tilde{w}$, Equation (14)] are solved as a function of x in terms of the joint parameters and the yet to-be-determined induced moment boundary conditions, $\overline{M}_1$ and $\overline{M}_2$. The determination of these moments is described in the following sections.

DETERMINING $\overline{M}_1$ AND $\overline{M}_2$

Shear- and peel-stress profiles along the joint can be calculated if $\bar{M}_1$ and $\overline{M}_2$ are known. Because the joint is statically indeterminate (see Figure 5), these moment reactions cannot be solved *a priori* using statics and geometric eccentricity. Furthermore, compatibility equations to solve for the redundant moment reaction requires the solution of the load transfer between adherends, which is what is being sought-and, therefore, such an approach is not possible. $\overline{M}_1$ and $\overline{M}_2$ can,

however, be found by iteration, subject to the condition that the predicted adhesive stress profiles satisfy force equilibrium. Comparison with FEA is needed to find out the best values of these two unknowns. Later, it is shown that $\overline{M}_1$ and $\overline{M}_2$ can be determined *a priori* by material and geometric parameters.

Two-dimensional full-integration plane strain four-node elements CPE4 in ABAQUS [19] were used to model joints having the same boundary conditions as specified in Figure 5. Six elements were used through the adhesive thickness. Although material behavior was limited to the linearly elastic regime, nonlinear geometric effects were accounted for. The joint parameters in Table 1 were used for FEA modeling. Overall and close-up views of the mesh are shown in Figure 6. Note that this FEA model includes a small amount of unbonded adherend regions at both sides of the joint, which are not included in the analytical model, shown in Figure 4. Both boundaries of the adherends were fixed against rotation and uniform x-direction displacement was applied at the right boundary of adherend 1. The right boundary of adherend 1 can freely translate along the z direction, whereas the left boundary of adherend 2 was fixed in all degrees of freedom. Shear- and peel-stress values were taken from the path along the adhesive midplane.

The results of the FEA are used to determine appropriate values for $\overline{M}_1$ and $\overline{M}_2$ in the analytical model (later, it will be shown that $\overline{M}_1$ and $\overline{M}_2$ can be specified without FEA). It was found that there is a unique constant $\overline{M}_{\mathrm{TOT}} = |\overline{M}_1| + |\overline{M}_2|$ that always satisfies equilibrium of shear stress in the joint (*i.e.*, integration of shear stress balances N_x):

$$\int_{-c}^{c} \tau_a dx = N_x. \tag{45}$$

Hence, $\overline{M}_1$ and $\overline{M}_2$ are related to each other. Note that $\overline{M}_2$ is a negative quantity for tensile loading N_x (see Figure 4). A positive

TABLE 1 Joint Parameters and Load for Single Lap Joint ($t_2/t_1 = 2$)

Joint parameters	Value
t_1 (mm)	1.24
t_2 (mm)	2.48
t_a (mm)	0.33
E_1, E_2 (GPa)	27.7
D_1 (N · mm)	4.40×10^{-3}
D_2 (N · mm)	35.2×10^{-3}
G_a (GPa)	0.927
N_x (MN/mm)	17.5

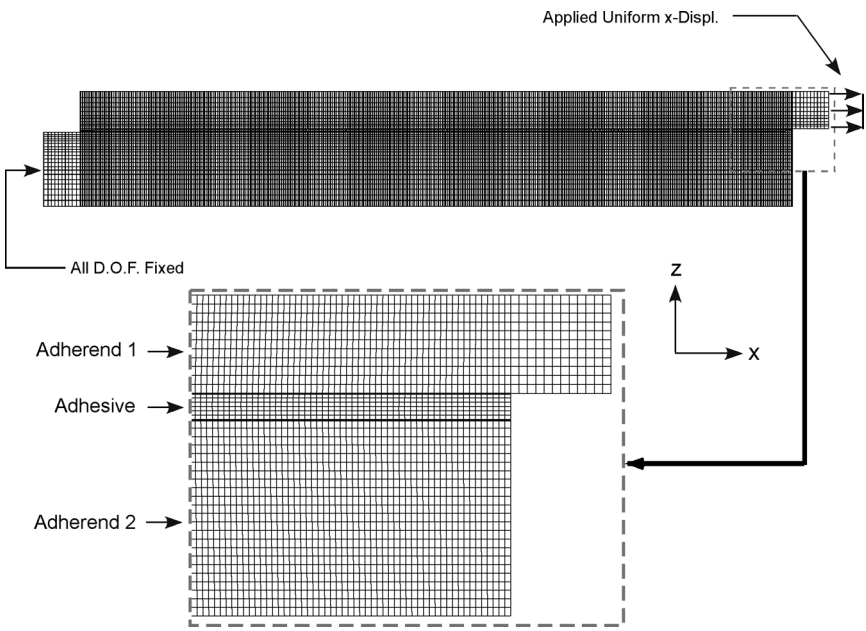

FIGURE 6 FEA mesh.

independent variable, Δ, is introduced to relate $\overline{M}_1$ and $\overline{M}_2$ with $\overline{M}_{\text{TOT}}$:

$$\overline{M}_1 = \Delta \cdot \overline{M}_{\text{TOT}} \tag{46}$$

and

$$\overline{M}_2 = \overline{M}_{\text{TOT}}(\Delta - 1). \tag{47}$$

$\overline{M}_{\text{TOT}}$ should, therefore, be first established, and that can be done by simply setting either $\overline{M}_1$ or $\overline{M}_2$ to zero. Once $\overline{M}_{\text{TOT}}$ is found, $\overline{M}_1$ and $\overline{M}_2$ are determined by varying Δ and comparing the resulting peel- and shear-stress predictions with the FEA results. For example, when the applied tension load, N_x, is 17.5 MN/mm, $\overline{M}_{\text{TOT}}$ was 49.0 MN/mm. Only this unique value of $\overline{M}_{\text{TOT}}$ will satisfy Equation (45) for any combination of $\overline{M}_1$ and $\overline{M}_2$. Δ is defined to a ratio of $\overline{M}_1$ over $\overline{M}_{\text{TOT}}$ and will vary from 0 to 1. Δ is varied incrementally between 0 to 1 and the calculations are repeated until the shear and peel stress profiles are best matched by minimization of the error functions:

$$\text{Error 1} = \sum_{i=1}^{N} \left[\sigma_p^{\text{FEA}}(x_i) - \sigma_p^{\text{AS}}(x_i) \right]^2 \tag{48}$$

and

$$\text{Error } 2 = \sum_{i=1}^{N} \left[\tau_a^{\text{FEA}}(x_i) - \tau_a^{\text{AS}}(x_i) \right]^2. \tag{49}$$

In Equations (48) and (49), the superscript AS refers to the analytical solution (AS). The AS has been divided into N discrete points, matching the location of points extracted from the FEA solution. Because the FEA is a linearly elastic model, the corner locations at the adhesive–adherend interfaces are actually stress singularity points. Also, the shear stress profile from the FEA satisfies the traction-free boundary condition at both ends of the joint, whereas the shear-lag-based analytical predictions cannot satisfy this condition. For these reasons, error functions comparing the stresses over the entire solution domain have been used in choosing end moment values, resulting in best matching shear- and peel-stress profiles, rather than simply comparing the solutions at the ends of the overlap. This approach is justified because the singular region composes less than 1% of the solution domain for realistic adhesive bondline thickness.

In Figure 7, the error functions 1 and 2 are plotted for a Δ increment of 0.05. A summation of error function 1 and 2 is defined as $\text{Error}_{\text{sum}}$ and plotted with respect to the variation of Δ. The minimum point of this $\text{Error}_{\text{sum}}$ function is chosen as the best match of the analytical peel- and shear-stress predictions with the FEA results. In Figure 8, the shear- and peel-stress profiles corresponding to the best match choice of Δ ($\Delta = 0.13$ for this test case) are plotted. Note that $\tau_a(x)$ and $\sigma_p(x)$ are normalized with respect to average shear stress:

$$\tau_{\text{ave}} = \frac{N_x}{2c}. \tag{50}$$

From Figures 7 and 8, it is clear that other criteria for choosing Δ would yield a better fit to the τ_a profile at the cost of a worse fit to the peel stress. The methodology presented herein, however, always results in an overprediction of both τ_a and σ_p stresses and can, therefore, be considered as conservative.

This methodology for determining the best choice of Δ always requires some baseline profile for comparison, namely FEA. Because having to generate a FEA model to find the $\overline{M}_1$ and $\overline{M}_2$ boundary conditions negates the benefit of having a closed-form model, a simple relationship is now sought between simple geometrically calculated moments, and the moment boundary conditions $\overline{M}_1$ and $\overline{M}_2$. Geometric moments M_1 and M_2 based on a zero adhesive-thickness

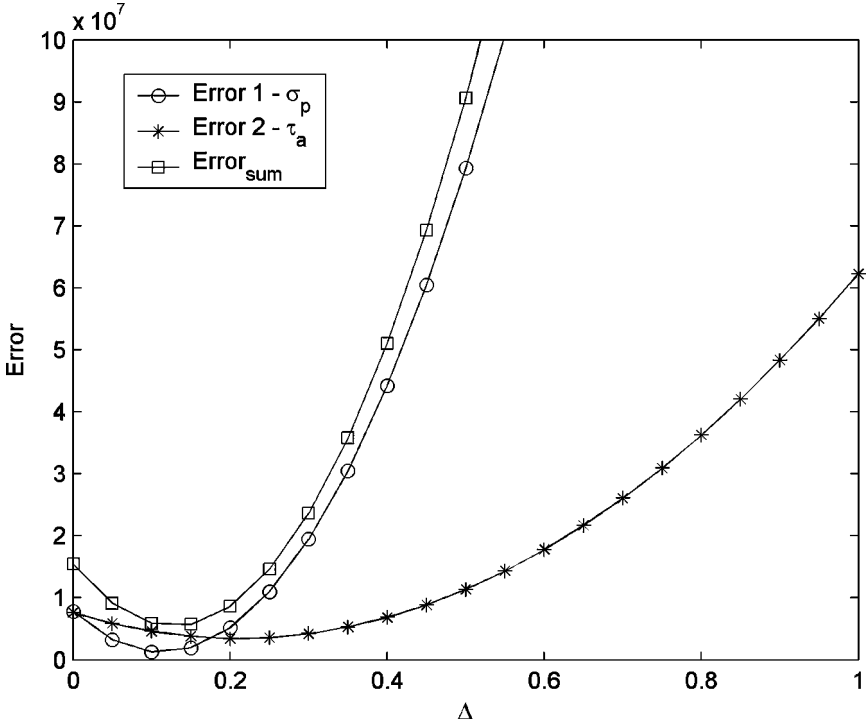

FIGURE 7 Error functions *versus* Δ.

geometry are chosen to establish this relationship. The choice of neglecting the adhesive thickness has been made because the BOEF peel-stress solution does account for t_a:

$$M_1 = \frac{N_x}{2} t_1 \tag{51}$$

and

$$M_2 = -\frac{N_x}{2} t_2. \tag{52}$$

Comparison of $\overline{M}_1$ and $\overline{M}_2$, found by this process (relying on FEA), with M_1 and M_2 over a wide range of asymmetric joints ($t_1 \neq t_2$ and $E_1 \neq E_2$), is shown in Table 2. Note that the thickness and modulus of adherend 2 are fixed in Table 2; $t_2 = 2.48\,\text{mm}$ and $E_2 = 27.7\,\text{Gpa}$. This comparison is accomplished in two ways: (1) independently varying adherend 1 thickness, t_1, with respect to adherend 2 thickness, t_2, while E_1 is equal to E_2, or (2) independently varying adherend 1

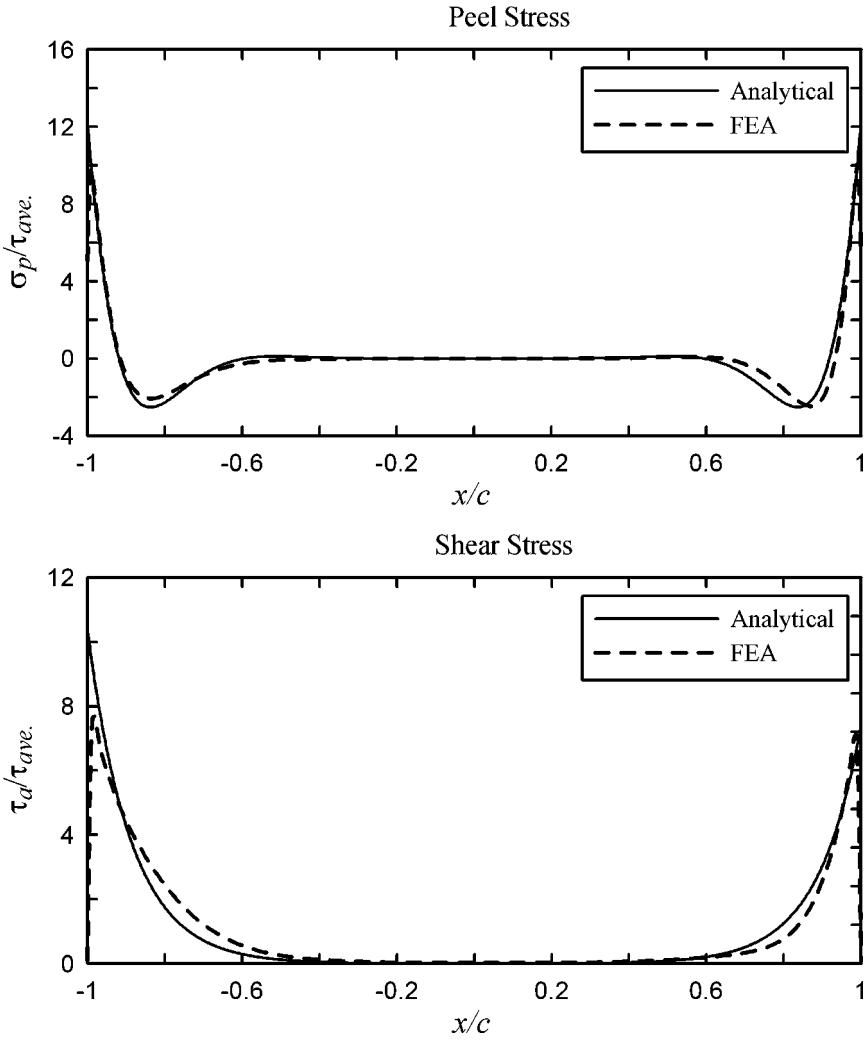

FIGURE 8 Best-fitted peel and shear stress profiles to FEA; asymmetric joint, $t_2 = 2t_1$.

Young's modulus, E_1, with respect to adherend 2 Young's modulus, E_2, while t_1 is equal to t_2. The following general relationship between the moments has been found by direct comparison of $\overline{M}_1$ with M_1 and $\overline{M}_2$ with M_2:

$$\overline{M}_1 = \xi \cdot M_1 \tag{53}$$

TABLE 2 $\overline{M}_1$ and $\overline{M}_2$ *versus* M_1 and M_2

	$\overline{M}_1$ (MN · mm)	$\overline{M}_2$ (MN · mm)	M_1 (MN · mm)	M_2 (MN · mm)
$E_1 = E_2$:				
$t_1 = 3t_2$	198	−7.28	65.1	−21.7
$t_1 = 2t_2$	87.1	−11.0	43.4	−21.7
$t_1 = t_2/2$	5.54	−43.5	10.8	−21.7
$t_1 = t_2/3$	2.43	−65.4	7.23	−21.7
$t_1 = t_2$:				
$E_1 = 3E_2$	37.7	−12.6	21.7	−21.7
$E_1 = 2E_2$	30.8	−15.4	21.7	−21.7
$E_1 = E_2/2$	15.5	30.5	21.7	−21.7
$E_1 = E_2/3$	12.7	−37.5	21.7	−21.7

and

$$\overline{M}_2 = \frac{1}{\xi} \cdot M_2 \tag{54}$$

where

$$\xi = \left(\frac{E_1}{E_2}\right)^{1/2} \frac{t_1}{t_2}. \tag{55}$$

Now, the moment boundary conditions $\overline{M}_1$ and $\overline{M}_2$ can be computed *a priori* using the geometric moments, as shown in Equations (53) and (54).

CASE STUDIES

The closed-form solution is demonstrated using three example calculation case studies. The first case study is a symmetric joint, $E_1 = E_2$ and $t_1 = t_2$. The second case study is an asymmetric joint with only adherend-thickness mismatch, $t_1 = t_2/3$ and $E_1 = E_2$. The last case study is an asymmetric joint with only adherend-modulus mismatch, $E_1 = E_2/3$ and $t_1 = t_2$. These parameters are listed in Table 3.

For each case study, the normalized peel- and shear-stress profiles are plotted in Figures 9–11 and compared with the corresponding FEA results taken along the adhesive midplane. In all FEA models, shear-stress profiles satisfy the zero traction condition at both free ends of the joint. Note that this condition cannot be satisfied from the shear-lag-based analytical predictions because of the way shear strain is calculated [see Equation (7)]. Therefore, the analytical method that predicts maximum shear- and peel-stresses at both free ends

TABLE 3 Joint Parameters for Single Lap Joint Case Studies

Joint parameters	Case I: symmetric joint	Case II: $t_1 = 1/3\ t_2$	Case III: $E_1 = 1/3\ E_2$
t_1 (mm)	2.48	0.83	2.48
t_2 (mm)	2.48	2.48	2.48
t_a (mm)	0.33	0.33	0.33
E_1 (GPa)	27.7	27.7	9.23
E_2 (GPa)	27.7	27.7	27.7
D_1 (N · mm)	3.5×10^{-2}	1.3×10^{-3}	1.2×10^{-2}
D_2 (N · mm)	3.5×10^{-2}	3.5×10^{-2}	3.5×10^{-2}
G_a (GPa)	0.927	0.927	0.927
N_x (MN/mm)	17.5	17.5	17.5

generally overpredicts stress values at these locations, relative to the FEA calculations. The symmetric case matches the FEA solution closely, whereas the asymmetric cases analyzed deviate more. Mismatches in adherend thickness result in more overprediction than modulus asymmetry.

As expected, the symmetric case (Figure 9) predicts symmetric shear- and peel-stress profiles about $x = 0$. The two asymmetric cases both involve increasing the stiffness of adherend 2, while keeping adherend 1 the same. In both cases, the peel-stress profile is predicted to be almost symmetric (see Figures 10 and 11). However, for $t_2 = 3t_1$ (Figure 10), the shear stress is predicted to be higher at $x = -c$ than at $x = c$. This result is the opposite of what the simple shear lag models (without bending effect) would predict. For $E_2 = 3E_1$, the maximum shear stress occurs at $x = c$, as expected per simple shear lag models. Because the thickness of the adherends affects their bending stiffness at a faster rate than the modulus, this reversal of behaviors can be attributed to bending effects. Such effects clearly must be accounted for in single lap joint analysis.

JOINT FAILURE PREDICTION

In the previous sections, an applied load, N_x, was chosen such that no yielding occurs within the adhesive. The constitutive behavior of a typical structural epoxy adhesive is plotted in Figure 12 together with an equivalent elastic/perfectly plastic constitutive curve. Equivalency is defined such that the area below the elastic/perfectly plastic curve is equal to the area below the experimentally measured stress-strain curve, or $A_1 = A_2$ in Figure 12. Based on this criterion, the shear yield stress, τ_y, can be selected for adhesives that do not show distinct

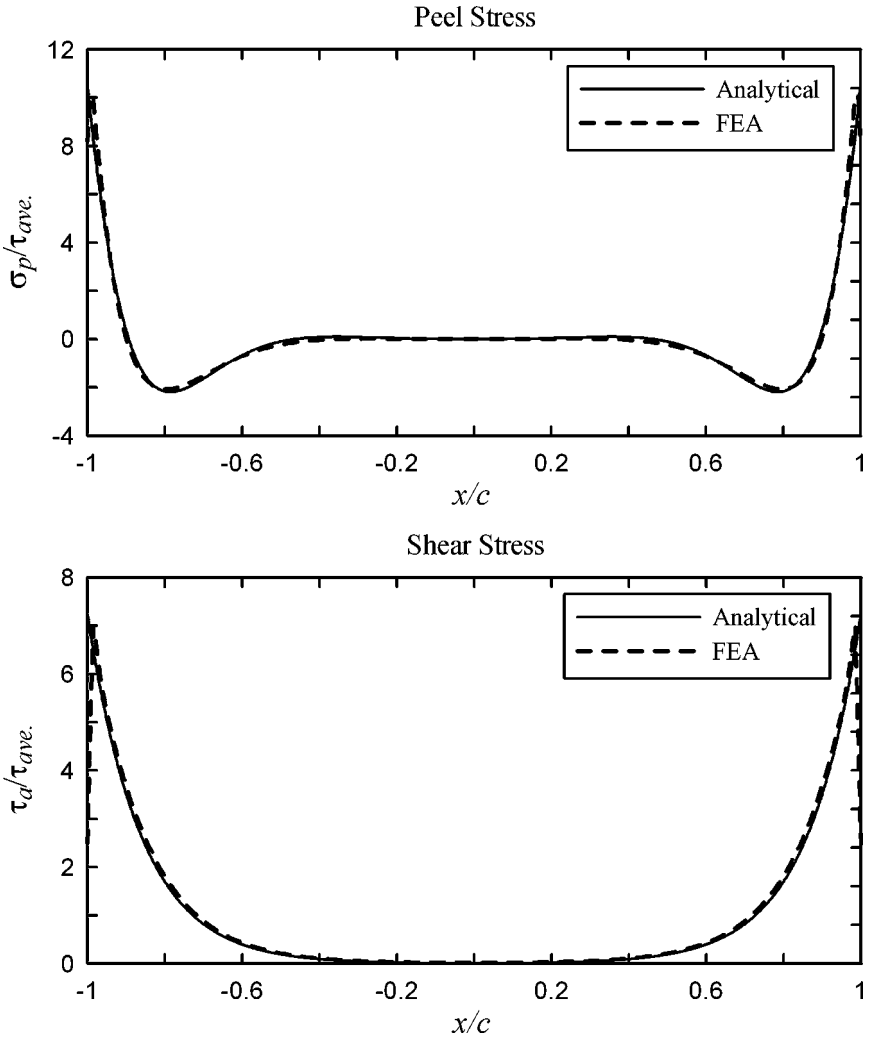

FIGURE 9 Peel and shear stress profiles for Case I: symmetric joint.

yielding behavior. Evaluation of joint failure, based on the adhesive reaching this elastic limit, must account for both the shear- and peel-stress components. For this purpose, the von Mises yield criterion is used:

$$3\tau_a^2 + \sigma_p^2 \leq 3\tau_y^2. \tag{56}$$

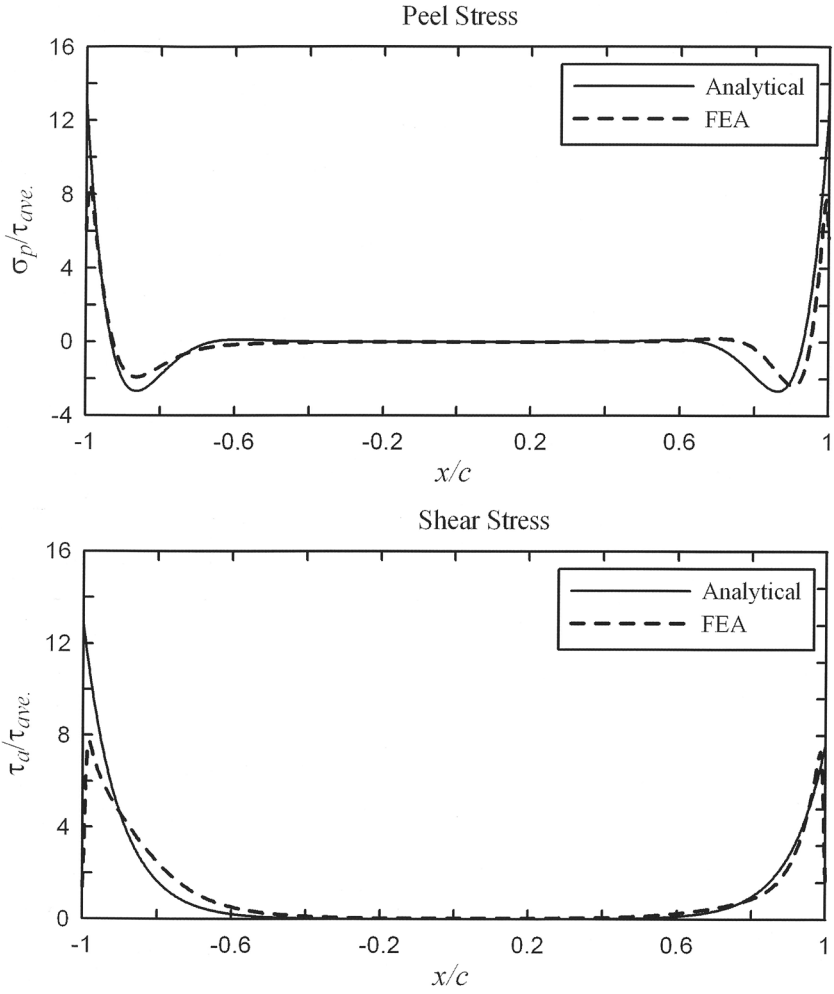

FIGURE 10 Peel and shear stress profiles for Case II: asymmetric joint, $t_2 = 3t_1$.

This criterion would be applied at locations $x = c$ and $x = -c$, where τ_a and σ_p are maximum. For asymmetric joints, yielding will generally occur on one side of the joint first. The applied load N_x associated with the onset of yielding is defined as the elastic limit load N_f.

The effect of in-plane stiffness ratio, E_1t_1/E_2t_2, on the elastic limit load is investigated over the range $0.01 \leq E_1t_1/E_2t_2 \leq 20$. This range

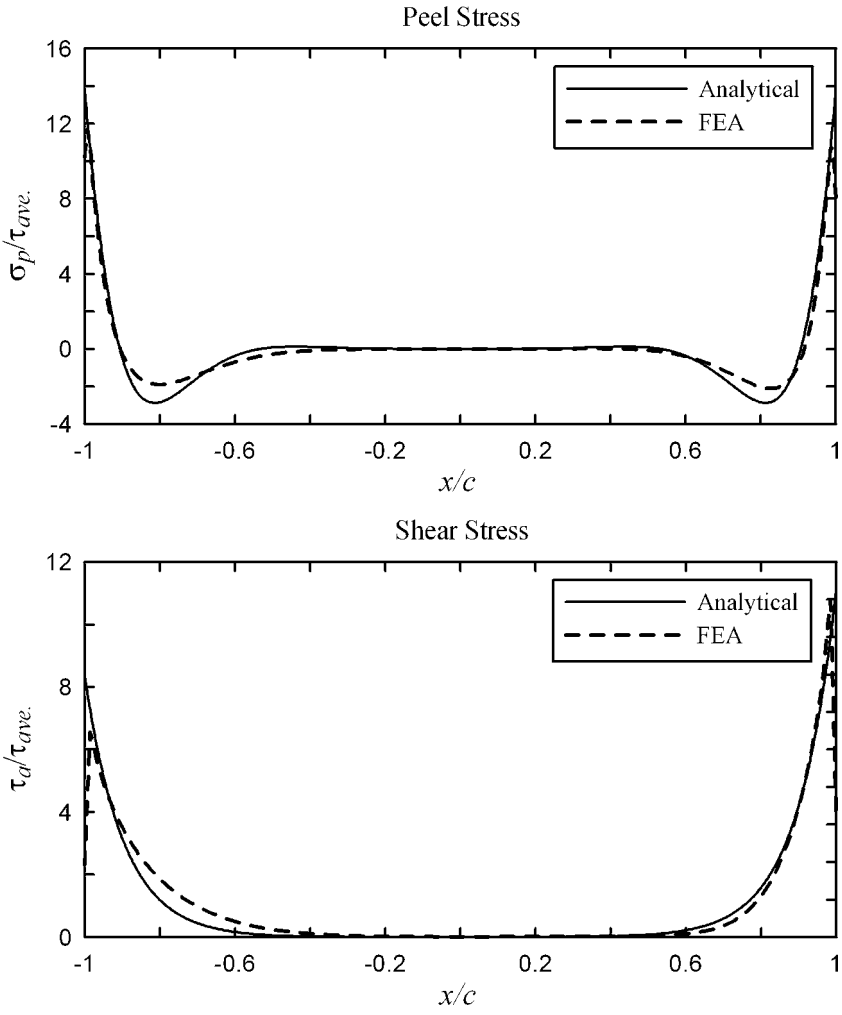

FIGURE 11 Peel and shear stress profiles for Case III: asymmetric joint, $E_2 = 3E_1$.

is accomplished in two ways: (1) independently varying adherend 1 thickness, t_1, while keeping E_1 and the product E_2t_2 constant, or (2) independently varying adherend 1 Young's modulus, E_1, while keeping t_1 and the product E_2t_2 constant. The anchor point for the range of joint parameters investigated is the symmetric joint case, where $E_1 = E_2$, and $t_1 = t_2$, as listed in Table 3, with adhesive behavior

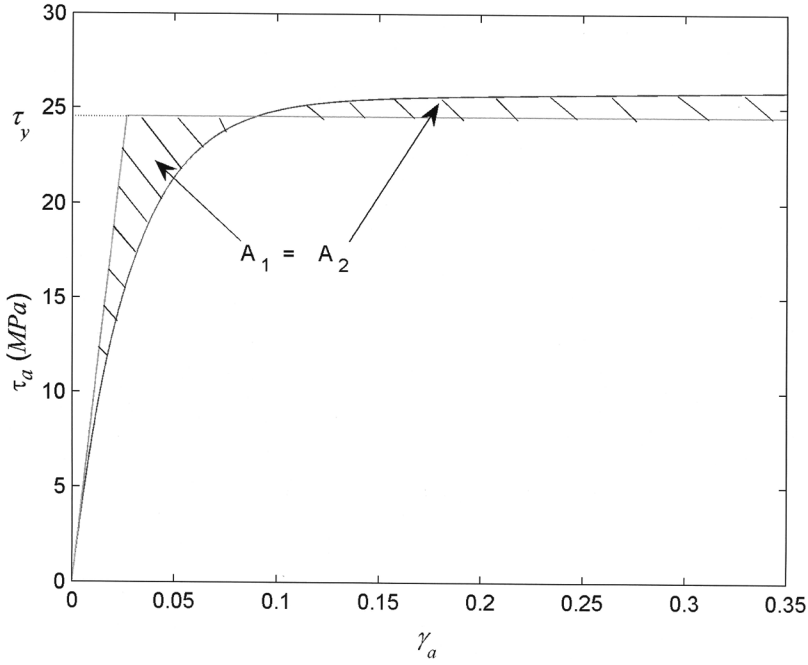

FIGURE 12 Constitutive behavior of typical epoxy adhesive.

summarized in Figure 12. The elastic limit load, N_f, is plotted as a function of stiffness ratio in Figures 13 and 14 for t_1 and E_1 variation, respectively. Within each plot are separate contours expressing different combinations of individual E_2 and t_2 values such that the product E_2t_2 remains a constant value of 68.7 kN/mm. The variable n in these plots is a scale factor on the thickness t_2, relative to the baseline 2.48-mm value for a symmetric joint ($n = 1$ and $E_1t_1/E_2t_2 = 1$). Accordingly, the modulus E_2 is scaled by $1/n$ so as to maintain a constant product E_2t_2.

In Figure 13, investigating the effect of changing t_1, N_f is found to increase as t_1 is increased for any set of E_2 and t_2 (*i.e.*, contours of n). This is due to the increase in stiffness of either adherend generally causing a reduction in the peak stresses at $x = \pm c$ as a result of a more evenly distributed shear stress profile. For any given stiffness ratio, there exists an optimum thickness for adherend 2, as indicated by the cusp in each contour. For example, for a joint with $E_1t_1/E_2t_2 = 0.333$, the strongest joint would be one with $n = 0.5$ (*i.e.*, $t_1 = 0.827$ mm, $E_1 = 27.7$ GPa, $t_2 = 1.24$ mm, and $E_2 = 55.4$ GPa). This

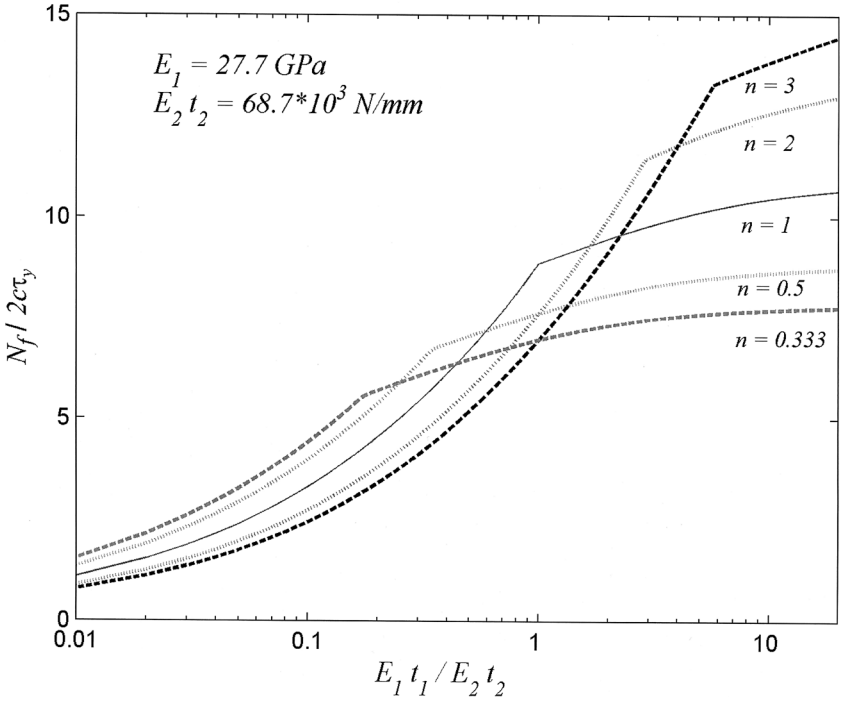

FIGURE 13 Elastic limit load for t_1 variation.

cusp exists because the changing location at which the yielding of the adhesive is predicted to occur. To the right of the cusp, yielding occurs at $x = c$, while to the left, yielding occurs at $x = -c$. At the cusp itself, yielding would occur simultaneously at both sides of the joint. Finally, in Figure 13, stronger joints are achieved over the range of changing t_1 values by proportionally adjusting t_2: higher n for increasing t_1, and lower n for decreasing t_1.

N_f is found to increase when independently increasing E_1, as indicated in Figure 14, for any set of E_2 and t_2 (*i.e.*, contours of n) because of the same reasons mentioned previously related to increasing adherend in-plane stiffness. Optimum joints are clearly identified by the cusps in each contour for each E_1t_1/E_2t_2 ratio. Stronger joints are achieved over the range of changing E_1 values by proportionally adjusting E_2 (lower n for increasing E_1 and higher n for decreasing E_1). For the case of varying E_1 to change the E_1t_1/E_2t_2 ratio, failure locations to the left and right of the cusp points in Figure 14 are the reverse of the thickness (t_1)-based sweep in stiffness ratio. Locations

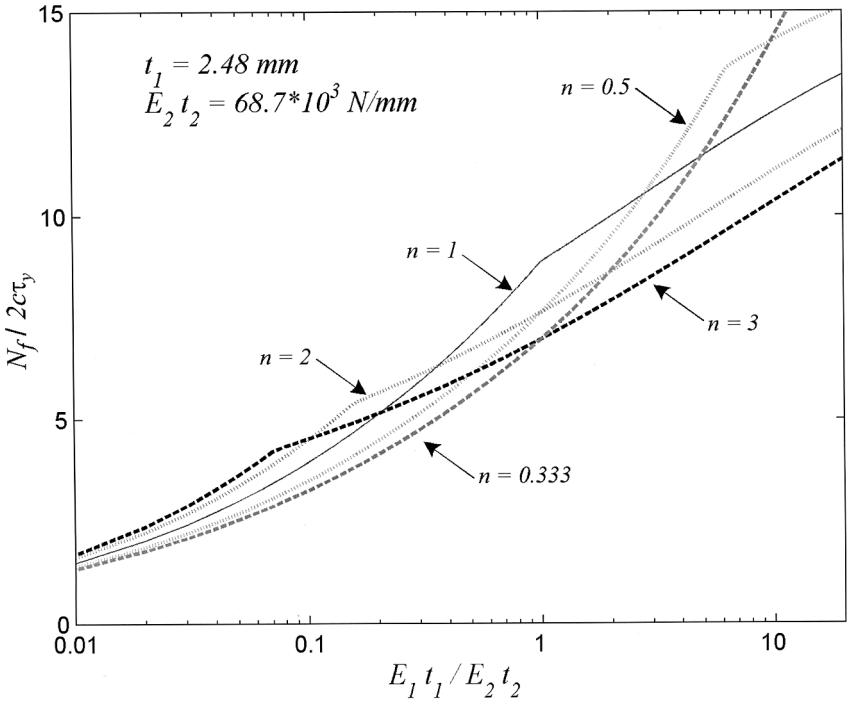

FIGURE 14 Elastic limit load for E_1 variation.

to the left of the cusps indicate failure at $x = c$, while to the right, failure occurs at $x = -c$. This reversal was observed in the previous case studies for which shear and peel stresses are plotted in Figures 10 and 11.

Figures 13 and 14 show that the thickness and modulus of the adherends independently affect joint strength, whereas purely shear-lag-based analyses [1, 2] that do not account for adherend bending effects predict that the elastic-limit load would scale only with the in-plane stiffness (product of thickness and modulus) and, thereby, would predict that the different contours in Figures 13 and 14 would collapse into a single trend. Therefore, the strength of the joint depends on both the in-plane stiffness as well as the bending stiffness of the adherends.

CONCLUSIONS

A closed-form model to predict the shear- and peel-stress profiles for a generally asymmetric single lap joint has been derived based on a coupled shear lag and beam-on-elastic-foundation

model. The following conclusions can be made based on the analysis results:

1. The self-induced eccentricity moment boundary conditions are a crucial component for accurate shear- and peel-stress prediction. Numerical empirical relationships between these eccentricity moments and statically calculated geometric moments are found and verified by FEA case studies.
2. The closed-form model predictions of peel- and shear-stress profiles are most accurate for symmetric joints. For asymmetric joints, the model predictions are more accurate for modulus eccentricity than for thickness eccentricity.
3. Cases analyzed show that the closed-form model always overpredicts maximum values of shear and peel stress relative to FEA near the free ends of the joint. This is due to the limitations of the shear-lag-based model, which does not satisfy the traction-free boundaries at the adhesive-free surfaces. In practice, there will always exist a spew fillet of adhesive and, thus, the shear stress does not need to truly go to zero at the joint ends. Finally, the overprediction of shear and peel stresses insures that this model will always make conservative predictions.
4. Failure of the joint is found to be strongly dependent on both the in-plane stiffness and bending stiffness of the adherends. The analysis developed herein allows for one to account for asymmetric joints in closed form, thereby aiding in seeking optimal joint configurations. The model predicts location of initial yielding of the adhesive depending on whether asymmetry exists as a result of thickness or material modulus differences.

REFERENCES

[1] Volkersen, O., Die Niektraftverteilung in Zugbeanspruchten mit Konstanten Laschenquerschritten, *Luftfahrtforschung* **15**, 41–47 (1938).
[2] Hart-Smith, L. J., Adhesive-bonded double-lap joints, NASA-Langley Contract Report, NASA-CR-112235 (1973).
[3] Goland, M. and Reissner, E. The stresses in cemented joints, *J. Appl. Mechanics* **11**, A17–A27 (1944).
[4] Ojalvo, I. U. and Eidinoff, H. L. Bond thickness effects upon stresses in single-lap adhesive joints, *AIAA J.* **16**(3), 204–211 (1978).
[5] Oplinger, D. W., Effects of adherend deflections in single lap joints, *Int. J. Solids Structures* **31**(18), 2565–2587 (1994).
[6] Kline, A. R., Stress analysis of adhesively bonded joints, in *Proc. of the International Symposium on Adhesive Joints: Formation, Characteristics and Testings*, Plenum Press (New York), pp. 587–610 (1984).

[7] Hart-Smith, L. J., Further developments in the design and analysis of adhesive-bonded structural joints, in *Joining of Composite Materials, ASTM STP 749* (Minneapolis, MN), K. T. Kedward (Ed.) (ASTM, 1981), pp. 3–31.
[8] Yang, C., Huang, H., Tomblin, J. S., and Sun, W., Elastic-plastic model of adhesive-bonded single-lap composite joints, *J. Composite Materials* **38**(4), 293–309 (2004).
[9] Tsai, M. Y., Oplinger, D. W., and Morton, J., Improved theoretical solutions for adhesive lap joints, *Int. J. Solids Structures* **35**(12), 1163–1185 (1998).
[10] Kim, H., The influence of adhesive bondline thickness imperfections on stresses in composite joints, *J. Adhes.* **79**, 621–642 (2003).
[11] Delale, F., Erdogan, F., and Aydinoglu, M. N., Stresses in adhesively bonded joints: A closed form solution, *J. Composite Materials* **15**, 249–271 (1981).
[12] Yang, C. and Pang, S., Stress-strain analysis of single-lap joints under tension, *J. Engineering Materials Technology* **118**, 247–255 (1996).
[13] Bigwood, D. A. and Crocombe, A. D., Elastic analysis and engineering design formulae for bonded joints, *Int. J. Adhesion Adhesives* **9**, 229–242 (1989).
[14] Mortensen, F. and Thomson, O. T., Coupling effects in adhesive bonded joints, *Composite Structures* **26**, 165–174 (2002).
[15] Wu, Z. J., Romeijn, A., and Wardenier, J., Stress expressions of single-lap adhesive joints of dissimilar adherends, *Composite Structures* **38**(1–4), 273–280 (1997).
[16] Tong, L., Bond strength for adhesively-bonded single-lap joints, *Acta Mechanica* **117**, 101–113 (1996).
[17] Fernlund, G., Papini, M., McCammond, D., and Spelt, J. K., Fracture load predictions for adhesive joints, *Composite Science Technology* **51**, 587–600 (1994).
[18] Adams, R., Strength predictions for lap joints, especially with composite adherends, *J. Adhes.* **30**, 219–242 (1989).
[19] Hibbitt, Karlsson & Sorensen, Inc., ABAQUS 6.3 User's Manual, Vol. 1 (Rowtucket, RI, USA, 2003).

APPENDIX

Nondimensional terms used in the compact expression of the joint solution:

$$\theta_1 = e^{\beta c}\sin(\beta c), \tag{A1}$$

$$\theta_2 = e^{\beta c}\cos(\beta c), \tag{A2}$$

$$\theta_3 = e^{-\beta c}\sin(\beta c), \tag{A3}$$

$$\theta_4 = e^{-\beta c}\cos(\beta c), \tag{A4}$$

$$\theta_5 = \theta_3^3 + \theta_4^3 - \theta_1(\theta_3 - \theta_4)(\theta_1 - 2\theta_2) + \theta_3\theta_4(\theta_3 + \theta_4) - \theta_2^2(3\theta_3 + \theta_4), \tag{A5}$$

$$\theta_6 = -\theta_1^3 + \theta_2^3 + \theta_3(\theta_1 + \theta_2)(\theta_3 + 2\theta_4) + \theta_1\theta_2(\theta_1 - \theta_2) + \theta_4^2(3\theta_1 - \theta_2), \tag{A6}$$

$$\theta_7 = -\theta_3^3 + \theta_4^3 - \theta_2(\theta_3 + \theta_4)(2\theta_1 + \theta_2) + \theta_3\theta_4(\theta_3 - \theta_4) + \theta_1^2(\theta_3 - 3\theta_4), \tag{A7}$$

$$\theta_8 = \theta_1^3 + \theta_2^3 - \theta_4(\theta_1 - \theta_2)(2\theta_3 - \theta_4) + \theta_1\theta_2(\theta_1 + \theta_2) - \theta_3^2(\theta_1 + 3\theta_2), \tag{A8}$$

and

$$\theta_9 = 2\beta^2[\theta_1^4\theta_3^4 + \theta_2^4\theta_4^4 + 2(\theta_1\theta_2 + \theta_3\theta_4)^2 - 2(\theta_1\theta_3 + \theta_2\theta_4)^2 - 6(\theta_1\theta_4 + \theta_2\theta_3)^2 + 4\theta_1\theta_2\theta_3\theta_4]. \tag{A9}$$

Constants C_1 to C_4 used with Equation (15):

$$C_1 = \frac{1}{\theta_9}\left[\theta_6\frac{\overline{M}_1}{D_1} - \theta_5\frac{\overline{M}_2}{D_2}\right], \tag{A10}$$

$$C_2 = \frac{1}{\theta_9}\left[\theta_8\frac{\overline{M}_1}{D_1} - \theta_7\frac{\overline{M}_2}{D_2}\right], \tag{A11}$$

$$C_3 = \frac{1}{\theta_9}\left[\theta_5\frac{\overline{M}_1}{D_1} - \theta_6\frac{\overline{M}_2}{D_2}\right], \tag{A12}$$

and

$$C_4 = \frac{1}{\theta_9}\left[\theta_8\frac{\overline{M}_2}{D_2} - \theta_7\frac{\overline{M}_1}{D_1}\right]. \tag{A13}$$

Integration constants C_5 and C_6 in Equations (34) and (35):

$$C_5 = \frac{1}{2\beta}\cos(\beta c)\left[e^{-\beta c}(-C_1 + C_2) + e^{\beta c}(-C_3 - C_4)\right] - \frac{1}{2\beta}\sin(\beta c)\left[e^{-\beta c}(C_1 + C_2) + e^{\beta c}(C_3 - C_4)\right] \tag{A14}$$

and

$$C_6 = -\frac{1}{2\beta}\cos(\beta c)\left[e^{\beta c}(-C_1 + C_2) + e^{-\beta c}(-C_3 - C_4)\right] - \frac{1}{2\beta}\sin(\beta c)\left[e^{\beta c}(C_1 + C_2) + e^{-\beta c}(C_3 - C_4)\right]. \tag{A15}$$

Constants C_7–C_{13} used in the adhesive shear strain solutions, Equations (41) and (42):

$$C_7 = \frac{1}{\lambda \sinh(2\lambda c)}[-\kappa_1 \cosh(\lambda c) + \kappa_2 \cosh(\lambda c)], \tag{A16}$$

$$C_8 = \frac{1}{\lambda \sinh(2\lambda c)}[\kappa_1 \sinh(\lambda c) + \kappa_2 \sinh(\lambda c)], \tag{A17}$$

$$C_9 = -\frac{2(C_1 + C_2)k\eta\beta^2 + (C_1 - C_2)k\eta\lambda^2}{2\beta(4\beta^4 + \lambda^4)}, \tag{A18}$$

$$C_{10} = \frac{2(C_1 - C_2)k\eta\beta^2 - (C_1 + C_2)k\eta\lambda^2}{2\beta(4\beta^4 + \lambda^4)}, \tag{A19}$$

$$C_{11} = \frac{2(C_3 - C_4)k\eta\beta^2 + (C_3 + C_4)k\eta\lambda^2}{2\beta(4\beta^4 + \lambda^4)}, \tag{A20}$$

$$C_{12} = \frac{2(C_3 + C_4)k\eta\beta^2 - (C_3 - C_4)k\eta\lambda^2}{2\beta(4\beta^4 + \lambda^4)}, \tag{A21}$$

and

$$C_{13} = -\frac{\zeta}{\lambda^2}. \tag{A22}$$

κ_1 and κ_2 are used in Equations (A16) and (A17):

$$\begin{aligned}\kappa_1 = &-\frac{N_x}{E_2 t_2 t_a} + \frac{t_2}{2D_2 t_a}\overline{M}_2 - \beta e^{-\beta c}[(C_9 + C_{10})\cos\beta c - (C_{10} - C_9)\sin\beta c] \\ &- \beta e^{\beta c}[(C_{12} - C_{11})\cos\beta c + (C_{11} + C_{12})\sin\beta c]\end{aligned} \tag{A23}$$

and

$$\begin{aligned}\kappa_2 = &\frac{N_x}{E_1 t_1 t_a} + \frac{t_1}{2D_1 t_a}\overline{M}_1 - \beta e^{\beta c}[(C_9 + C_{10})\cos\beta c + (C_{10} - C_9)\sin\beta c] \\ &- \beta e^{-\beta c}[(C_{12} - C_{11})\cos\beta c - (C_{11} + C_{12})\sin\beta c].\end{aligned} \tag{A24}$$